Stable coexistence of grandidierite and kornerupine during medium pressure granulite facies metamorphism

C. J. CARSON, M. HAND

School of Earth Sciences, University of Melbourne, Parkville, Victoria, 3052, Australia

AND

P. H. G. M. DIRKS

Department of Earth Sciences, University of Utrecht, P.O. Box 80.021, 3508TA, Utrecht, The Netherlands

Abstract

Petrological and mineral chemical data are presented for two new occurrences of co-existing borosilicate minerals in the Larsemann Hills, East Antarctica. The assemblages contain kornerupine and the rare borosilicate, grandidierite $(Mg,Fe)Al_3BSiO_9$. Two distinct associations occur: (1) At McCarthy Point, 1—10 mm thick tourmaline–kornerupine–grandidierite layers are hosted within quartzofeldspathic gneiss; and (2) Seal Cove, where coexisting kornerupine and grandidierite occur within coarse-grained, metamorphic segregations with Mg-rich cores of cordierite–garnet–spinel–biotite–ilmenite and variably developed plagioclase halos. The segregations are hosted within biotite-bearing, plagio-feldspathic gneiss. Textural relationships from these localities indicate the stability of co-existing kornerupine and grandidierite.

The grandidierite- and kornerupine-bearing segregations from Seal Cove largely postdate structures developed during a crustal thickening event (D_2) which was coeval with peak metamorphism. At McCarthy Point, grandidierite, kornerupine and late-tourmaline growth predates, or is synchronous, with F_3 fold structures developed during a extensive granulite grade, normal shearing event (D_3) which occurred prior to, and synchronous with, near-isothermal decompression. Average pressure calculations on assemblages that coexist with the borosilicates at Seal Cove, indicate the prevailing conditions were 5.2–5.5 kbar at $\sim 750°C$ for formation of the grandidierite-kornerupine assemblage.

KEYWORDS: grandidierite, kornerupine, decompression, coexisting borosilicates, Larsemann Hills, East Antarctica.

Introduction

GRANDIDIERITE is a Fe-Mg aluminous borosilicate $[(Mg,Fe)Al_3BSiO_9]$, and has been reported from around 20 localities world-wide (Lonker, 1988). Most reported occurrences are from low-pressure, high-temperature environments such as contact aureoles (e.g. Helmers and Lustenhouwer, 1988; Black, 1970; de Roever and Kieft, 1976) and in metasedimentary xenoliths within acid volcanics (van Bergen, 1980). However, grandidierite has also been reported within high-grade pegmatites from the Precambrian Metamorphic Complex of Rogaland, south-western Norway (Huijsmans et al., 1982, < 4 kbar at 700°C), and as a prograde or retrograde phase from several low- to medium-pressure granulite facies terrains including the Aldan Shield (Grew et al., 1989, 4.6–6.2 kbar at $\sim$ 750–800°C), the Canadian Shield of south-eastern Ontario (Lonker, 1988, 5.2-6.9 kbar at $\sim$ 700-760°C) and the Eastern Province Metamorphic Complex of Zambia (Vrána, 1979).

The low-pressure high-temperature paragenesis of grandidierite implied from the majority of field observations is supported by experimental evidence. Mg-grandidierite has been synthesized at $P_{H_2O} = 1$

kbar at temperatures in excess of 780°C (Olesch and Seifert, 1976). Rosenburg and Foit (1975) reported that at pressures of $\sim$ 1 kbar in the presence of excess B_2O_3 and H_2O, alkali-free tourmaline decomposes to grandidierite-quartz at temperatures greater than 750°C. Similar results were reported by Werding and Schreyer (1984) who showed that grandidierite is a product phase from the degeneration of alkali-free tourmaline at fluid pressures of between 1 and 2 kbar at 790° to 810°C respectively.

Although grandidierite formation appears favoured by very low-pressure and high-temperatures, several occurrences from higher pressure terrains have been described (e.g. Nicollet, 1990; van Bergen, 1980; Haslam,1980). In many cases, a problem in assessing the stability field of grandidierite from $P-T$ estimates is that grandidierite growth does not appear to have occurred during maximum pressure conditions, or the relationship between maximum pressures and grandidierite formation is inadequately described. Nicollet (1990) describes the occurrence of grandidierite in migmatitic gneisses in southern Madagascar, and suggests that grandidierite is associated with migmatization which occurred at 4−5 kbar and at 700°C. Grandidierite, however, occurs as inclusions within cordierite and garnet and may predate peak conditions. Haslam (1980) reports grandidierite from contact metamorphosed sediments from Malawi, from which pressures of between 3 and 6 kbar have been tentatively suggested. However, the relationship between the reported pressures and grandidierite growth is poorly constrained. Van Bergen (1980) discusses an occurrence of grandidierite from a granulite terrain in Norway first reported by Krogh (1975). In this case, assumed conditions for grandidierite growth are based on the crystallization conditions (9−11 kbar at 1000°C) for a late magmatic intrusion in the region. The exact relationship between this intrusion and timing of grandidierite growth in the host gneisses is unclear, and $P-T$ estimates from the intrusion may bear no relation to the conditions of formation of the grandidierite.

Kornerupine is a relatively uncommon Mg-Fe borosilicate reported from around 50 localities worldwide and is typically found in Si-poor, Mg-Al rich, upper amphibolite to mostly medium pressure (> 4 kbar), granulite-grade metamorphic rocks (e.g. Grew *et al.*, 1991*a*; Grew, 1982; Lonker, 1988; Ackermand *et al.*, 1991; Waters and Moore, 1985). It is often found in paragneiss sequences in association with Mg-aluminous associations such as sillimanite, sapphirine (but not sapphirine + quartz), orthopyroxene, cordierite and spinel and rarely with quartz and plagioclase. Experimental studies in the boron-free system, $MgO-Al_2O_3-SiO_2-H_2O$ [MASH] (Seifert, 1975), and the boron-bearing system,

$MgO-Al_2O_3-SiO_2-H_2O-B_2O_3$ [MASHB] (Robbins and Yoder, 1962), have placed quantitative constraints on the stability field of kornerupine. In the MASHB system, Robbins and Yoder (1962) reported the appearance of the assemblage kornerupine–sapphirine–liquid in experimental charges from degeneration of Mg-rich tourmaline (dravite) at 895°C and 5 kbar. Seifert (1975) synthesized boron-free kornerupine and established that boron-free kornerupine is stable to pressures above 4.5 kbar at temperatures greater than 735°C. Seifert (1975) and Grew *et al.* (1991*b*) suggested that the addition of B (and/or Na, Siefert, 1975) to the system may expand the stability field of kornerupine to higher temperatures. In MASHB, Werding and Schreyer (1978) showed that B-kornerupine was stable in excess of 7 kbar at 830°C, and further suggested that at high B_2O_3/H_2O ratios the coexistence of kornerupine with grandidierite and tourmaline is favoured.

Kornerupine–grandidierite $\pm$ tourmaline assemblages have rarely been described (Lonker, 1988), with occurrences of other combinations of borosilicates similarly infrequent (e.g. Vrána, 1979). Disequilibrium textures between grandidierite, tourmaline, kornerupine and Ti-dumortierite from felsic gneisses in Zambia, have been described by Vrána (1979). He considered grandidierite to be an early phase, pre-dating the growth of kornerupine. Ren *et al.* (1992) report a grandidierite–kornerupine–tourmaline assemblage from Storness Peninsula, in the Larsemann Hills, and note that grandidierite forms inclusions within kornerupine, suggesting grandidierite growth predates kornerupine. Grew *et al.* (1989, 1991) describe kornerupine-bearing slyudites from the Aldan Shield in which both grandidierite and tourmaline are considered to be post-peak mineral phases, associated with partial melting (Grew *et al.*, 1989). Similarly, Lonker (1988) describes kornerupine–grandidierite–tourmaline assemblages in migmatitic pelitic granulites from Ontario, Canada, with grandidierite formation occurring during decompressional heating and postdating kornerupine growth. However, in this case, no textural relationships between the borosilicates were observed.

Coexisting stable grandidierite and kornerupine assemblages are predicted by Lonker (1988) in the system KNFMASHB (with $PH_2O < P_{total}$). Lonker (1988) also suggests that the absence of coexisting grandidierite and kornerupine reported in nature may be due to the lack of sufficiently boron-enriched bulk compositions that would support coexisting borosilicates. To the authors' knowledge, grandidierite and kornerupine have never been described previously in the literature as stably coexisting phases. Grandidierite is invariably described as either

replacing, or as having been replaced by kornerupine during prograde or retrograde metamorphism, and that the metamorphic conditions prevailing during borosilicate growth (especially grandidierite) is often poorly constrained.

In this paper we document an occurrence of stably coexisting grandidierite–kornerupine from medium-pressure granulite facies psammitic and feldspathic gneisses in the Larsemann Hills, East Antarctica. These occurrences occur in two distinct lithological, mineralogical and structural associations. By utilising average pressure calculations after Powell and Holland (1994), using assemblages that coexist with the borosilicates, we constrain the $P-T$ conditions of coexisting grandidierite and kornerupine in the Larsemann Hills.

Regional geology

The Larsemann Hills are located on the Ingrid Christensen coastline of Prydz Bay, East Antarctica, and consist of a number of small ice-free peninsulas and offshore islands representing some 60 km^2 of exposure (Fig. 1). These outcrops form part of an extensive mid-Proterozoic (1100–1000 Ma) granulite facies terrain that covers much of East Antarctica (e.g. Sheraton et al., 1984; Sheraton et al., 1980; Black et al., 1987). The Larsemann Hills are dominated by migmatitic pelitic, psammitic and felsic paragneisses. These lithologies represent intra-basinal sediments that experienced low-medium pressure granulite facies metamorphism traditionally interpretated to have occured during this 1000–1100 Ma event (Sheraton et al., 1984; Stüwe and Powell, 1989).

Previously published estimates of peak-metamorphic conditions are ~ 4.5 kbar and 750°C, with post-peak metamorphic textures recording around 0.5–1.0 kbar of isothermal decompression (Stüwe and Powell, 1989). Somewhat higher peak conditions are reported by Ren et al. (1992) and Carson et al. (1995) with peak conditions of ~ 9 kbar and 850°C and ~ 7 kbar and 780°C respectively.

Recently, however, the age of granulite facies metamorphism in the Larsemann Hills has been questioned. Zhao et al., (1992) report a Pan-African age on a syn-deformational granite (547 ± 9 Ma using $^{207}Pb/^{206}Pb$ systematics on zircon) which lead
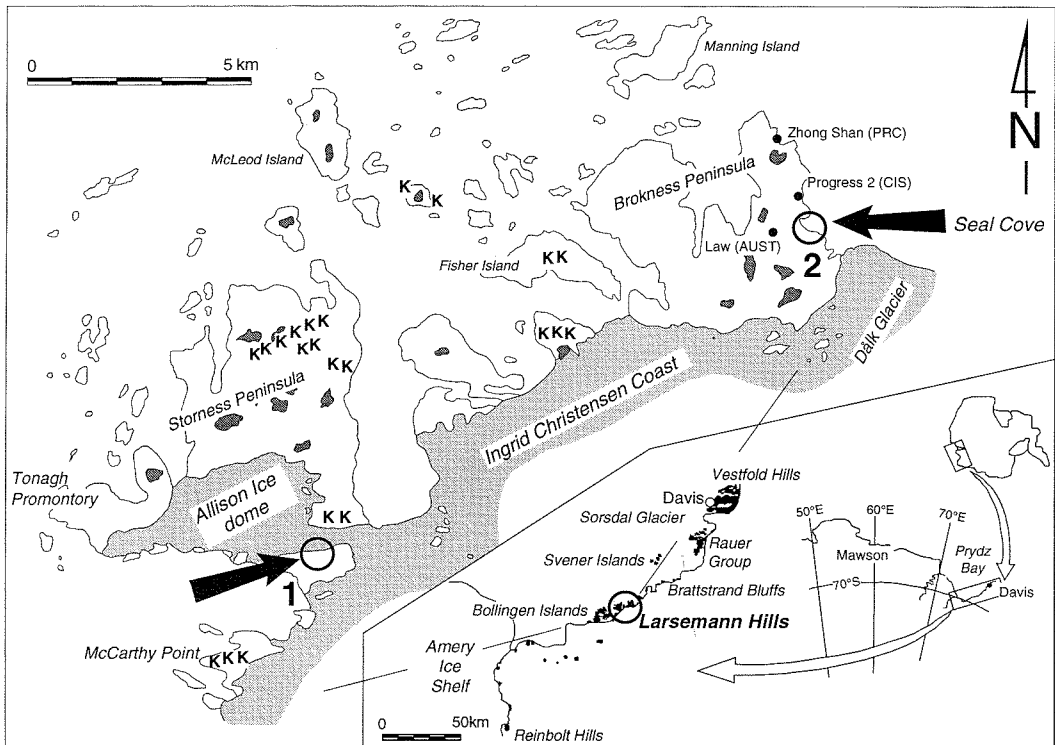

FIG. 1. Locality map of the Larsemann Hills showing the borosilicate sites described in the text. Site 1: McCarthy Point locality, Site 2: Seal Cove locality. Kornerupine localities are indicated by K. Inset: Location of Larsemann Hills on the Prydz Bay Coast.

Ren *et al.* (1992) to suggest that the pervasive deformation and associated metamorphism is Pan-African, rather than mid-Proterozoic, in age. Other workers have suggested two unrelated metamorphic peaks in the Larsemann Hills, one at ~ 1000 Ma and a later event at ~ 550 Ma at similar temperatures but somewhat lower pressure (e.g. Dirks *et al.*, 1993; Carson *et al.*, 1995), the interference of the two peaks giving the appearance of an isothermal decompression path.

Two major high-grade structural events in the Larsemann Hills have been identified (see Carson *et al.*, 1995, for further description on nomenclature of structures in the Larsemann Hills). The majority of the Larsemann Hills is dominated by D_2, during which the dominant foliation, S_2, was produced in response to regional NW directed thrusting. In outcrop, S_2 commonly forms a complexly folded form surface and is overprinted by numerous generations of co-linear F_2 folds. D_2 is synchronous with peak metamorphism. D_3 is characterized by the development of relatively planar high-strain zones that have a normal, south-down, shear sense. The zones contain a well developed south-plunging lineation and formed prior to, and synchronously with, the development of near-isothermal decompression textures. Good examples of D_3 high-strain zone domains are southern Storness Peninsula and the McCarthy Point area, south of the Allison Ice Dome (Fig. 1).

Petrography of grandidierite-bearing rocks

McCarthy Point locality. At McCarthy Point dark narrow (1–10 mm) borosilicate-rich domains define S_3 within a pale, medium-grained, granular, quartzofeldspathic gneiss. The host gneiss mineralogy consists of an equigranular polygonal matrix of plagioclase, quartz and minor K-feldspar and biotite.

The borosilicate layers consist predominantly of granular, fine-grained tourmaline with coarse, dark green kornerupine crystals that occur in radiating splays, up to 75 mm in length, within the layering (Fig. 2a). Euhedral kornerupine also occurs as aligned crystals in the axial plane of F_3 folds forming a weak axial plane S_3 foliation (Fig. 2b). Inclusions within the kornerupine include rounded tourmaline grains, zircon, ilmenite and rare graphite flakes. The borosilicate-rich layers are characteristically poor in biotite, in contrast to the enclosing quartzofeldspathic layers, and contain no other Mg-Fe bearing phases. Rare boudinaged kornerupine grains contain anhedral tourmaline growth within boudin necks. Where kornerupine occurs in quartz-plagioclase domains, the kornerupine crystals are strongly corroded and commonly separated from plagioclase by moats of retrograde quartz$_2$ (qtz_2, Fig. 3a). Grandidierite occurs in contact with quartz and plagioclase as corroded prismatic crystals and as rare symplectitic intergrowths with quartz. Retrograde quartz moats (qtz_2) between grandidierite and plagioclase are common (Fig. 3b). Ilmenite, and tourmaline are common inclusions phases. Grandidierite also mantles rare, corroded sillimanite. Grandidierite usually occurs co-existing with kornerupine (Fig. 3c,d) and, less commonly, as poikiloblastic intergrowths with the granular tourmaline.

Tourmaline occurs in two associations: tourmaline$_1$ (T_1) occurs as small, rounded inclusions within grandidierite and kornerupine; and tourmaline$_2$ (T_2) usually forms extensive equigranular polygon growths stable with matrix quartz and plagioclase. Inclusion phases within tourmaline$_2$ include rutile and ilmenite. Tourmaline$_2$ also forms thin, discontinuous coronas on grandidierite, but rarely on kornerupine (Fig. 3e), and occasionally mantles strongly corroded, sillimanite grains (Fig. 3f).
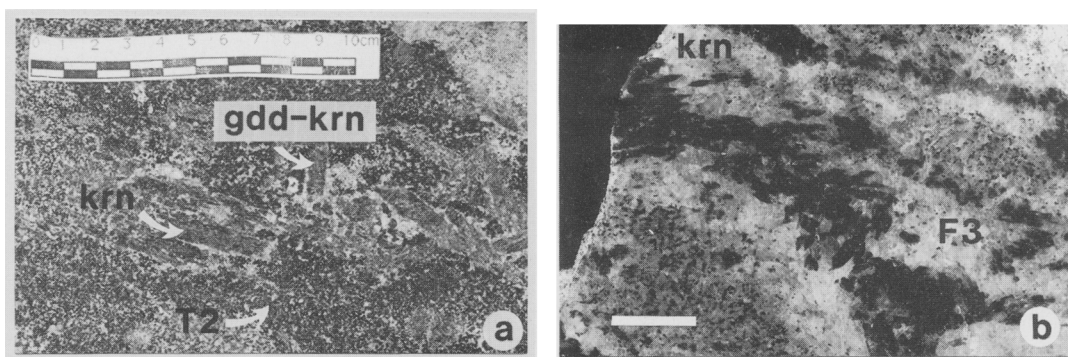

FIG. 2. McCarthy Point (*a*) kornerupine (krn)-grandidierite (gdd)-tourmaline$_2$ (T_2) layer in psammitic gneiss. Scale bar in cm. (*b*) Euhedral kornerupine aligned in axial plane of F_3 fold. Scale bar = 20 mm.
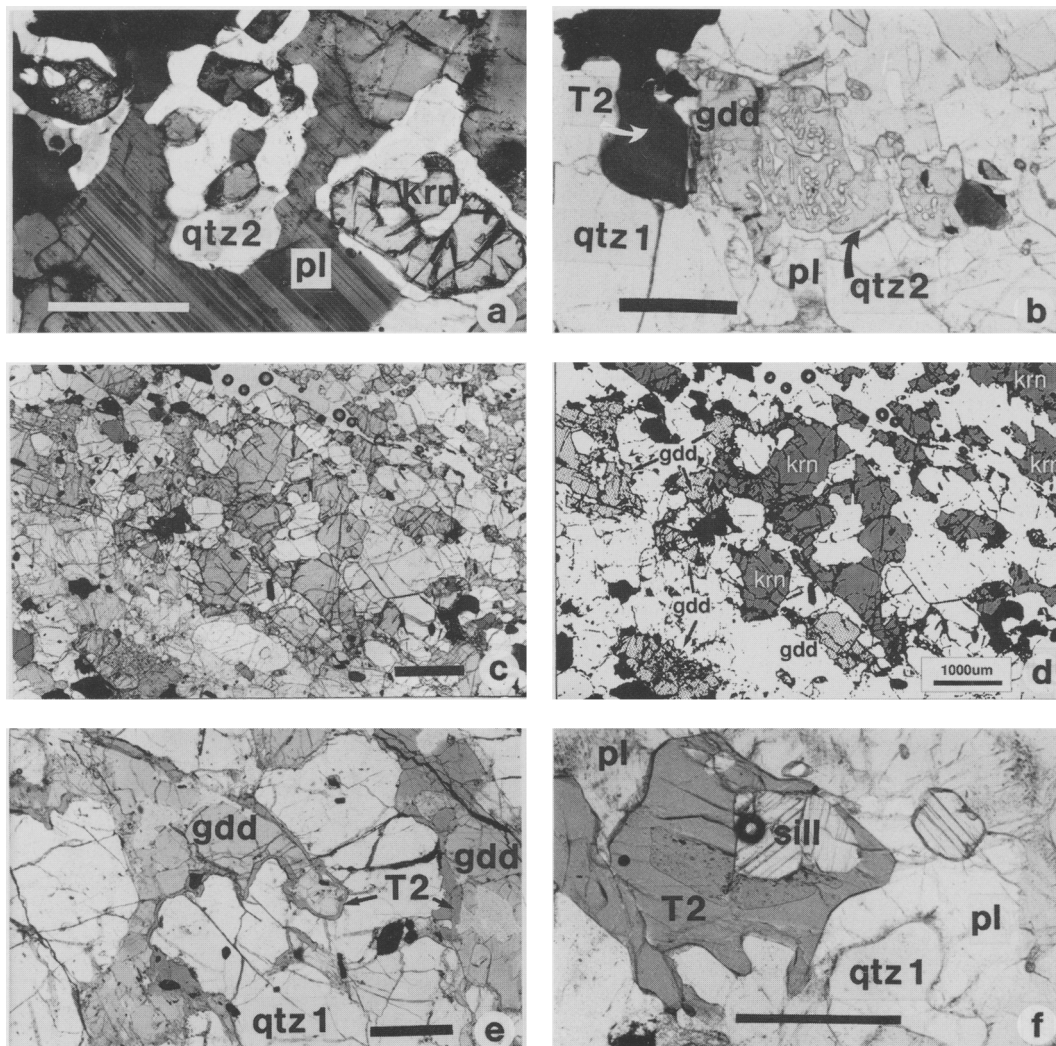
FIG. 3. Photomicrographs of McCarthy Point textures. (a) Corroded kornerupine mantled by quartz$_2$ (qtz$_2$) in contact with plagioclase (pl). Scale bar = 500 μm. (b) Grandidierite-quartz symplectite with moat of quartz$_2$ around grandidierite. Scale bar = 400 μm. (c) Kornerupine and grandidierite in contact. Scale bar = 1000 μm. (d) diagram of photomicrograph highlighting textural relationships in (c). (e) Grandidierite with corona forming tourmaline$_2$ (T$_2$). Scale bar = 700 μm. (f) Rare sillimanite (sill) mantled by tourmaline$_2$. Scale bar = 500 μm.

Seal Cove locality. At Seal Cove, the host lithology consists primarily of medium-grained equigranular plagioclase with biotite defining a well developed S$_2$ fabric with minor corroded spinel, ilmenite and rare rutile. Folded inclusion trails of sillimanite and rounded resorbed grains of quartz (qtz$_1$) occur as inclusion phases within plagioclase.

Grandidierite and kornerupine occur within concentrically arranged metamorphic segregations that contain a core consisting of kornerupine–

grandidierite–cordierite–garnet–biotite–spinel with minor ilmenite–rutile surrounded by a moat of granoblastic plagioclase (Fig. 4a). Garnet, ilmenite, biotite$_1$ and spinel (with coarse magnetite exsolution) are texturally early phases, and are present as resorbed grains enclosed within coarse cordierite and kornerupine intergrowths. Late biotite$_2$ is present as large euhedral unorientated crystals. Fine, radiating euhedral grandidierite needles occur as unorientated inclusions within cordierite, and as
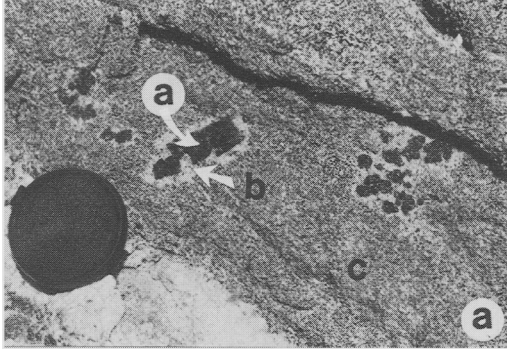
FIG. 4. Seal Cove. (a) Composite metamorphic segregation showing the general concentric arrangement of mineral phases: (a) Fe-Mg rich core phases ($\pm$ borosilicates), (b) biotite-absent plagioclase halo, and (c) biotite-bearing host feldspathic gneiss. Lens cap 50 mm diameter.

idierite needles also form narrow coronas on resorbed garnet, ilmenite and spinel (Fig. 5b,c). Rare, narrow retrograde quartz moats (qtz$_2$) are present between grandidierite grains and cordierite (Fig. 5d). Tourmaline is notably absent from the Seal Cove assemblages.

The host gneiss and nearby meta-pelitic and meta-psammitic lithologies under went extensive anatexis during high-grade metamorphism. Numerous garnet- and cordierite-bearing leucosomes occur and are synchronous with, and post-date, S$_2$ development. The leucosomes occupy the same structural position as the grandidierite–kornerupine-bearing segregations. Furthermore, segregation formation and melt generation appear closely related as there is a transition from individual mafic segregations with minor leucocratic halos to voluminous, igneous textured, K-feldspar-bearing pegmatites that transect the S$_2$ fabric.

Mineral chemistry

intergrowths within coarse subhedral kornerupine (Fig. 5a). Both kornerupine and euhedral grand-

Electron microprobe analyses were obtained with a Cameca Camebax-Microbeam SX-50, at the School
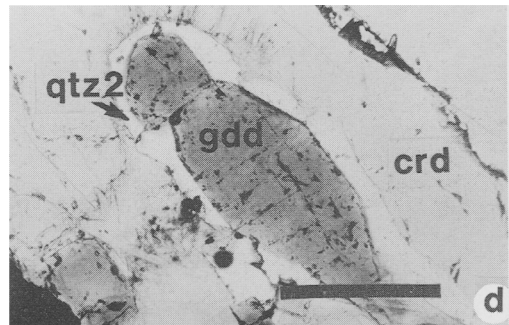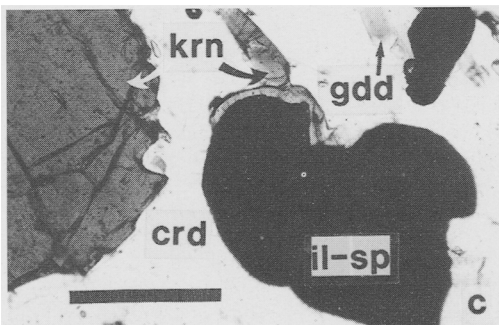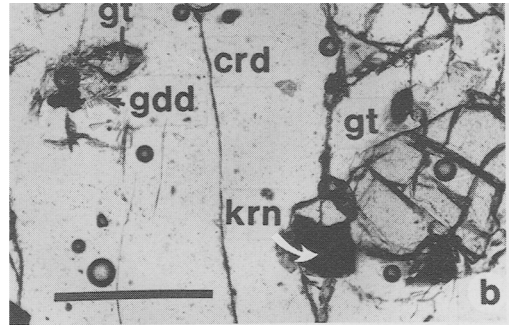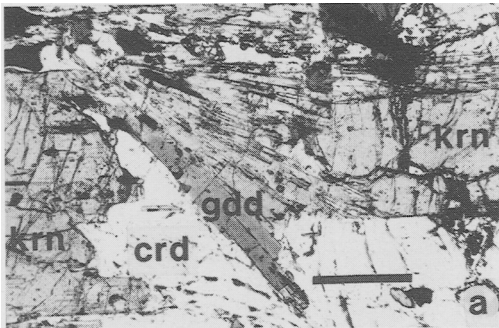
FIG. 5. Photomicrographs of Seal Cove textures. (a) grandidierite and kornerupine intergrowth within cordierite (crd) in segregation. Scale bar = 500 μm. (b) grandidierite and kornerupine growth on corroded garnet (gt). Scale bar = 500 μm. (c) grandidierite and kornerupine growth on ilmenite-spinel (il-sp). Scale bar = 500 μm. (d) quartz moats (qtz$_2$) between grandidierite and cordierite within segregation. Scale bar = 500 μm. Mineral abbreviations as in Figs 2 and 3.

TABLE 1. Selected mineral analyses from McCarthy Point

Oxide	grandidierite core	rim	kornerupine core	rim	tourmaline incl.	corona	plagioclase		sillimanite
SiO_2	19.68	19.86	29.32	29.62	34.91	34.45	61.96	62.63	35.97
Al_2O_3	50.76	50.81	41.05	41.09	31.28	31.76	22.59	22.51	62.51
TiO_2	0.00	0.12	0.19	0.28	2.09	0.92	0.03	0.00	0.00
MnO	0.02	0.07	0.04	0.07	0.04	0.02	0.00	0.00	0.03
FeO†	6.03	5.96	10.03	9.77	5.76	5.82	0.05	0.08	0.87
MgO	11.02	11.26	13.40	13.16	7.90	8.34	0.00	0.00	0.06
Cr_2O_3	0.05	0.02	0.06	0.02	0.07	0.04	0.00	0.00	0.00
CaO	0.03	0.01	0.03	0.03	1.31	1.28	4.07	4.01	0.01
K_2O	0.00	0.01	0.00	0.01	0.11	0.07	1.94	0.82	0.00
Na_2O	0.01	0.00	0.07	0.10	1.97	2.00	8.22	8.92	0.03
B_2O_3	11.96	11.46	5.21	4.22	9.67	9.27	n.d.	n.d.	n.d.
F*	0.01	0.08	0.66	0.64	0.43	0.34	0.00	0.00	0.00
Cl**	0.00	0.01	0.02	0.00	0.00	0.00	0.00	0.00	0.00
Total	99.57	99.67	99.81	98.73	95.35	94.18	98.86	98.97	99.57
No of O	9	9	22	22	31	31	8	8	20
Si	0.975	0.988	3.696	3.611	6.266	6.213	2.789	2.799	3.922
Al	2.965	2.968	6.104	5.894	6.622	6.766	1.198	1.185	8.032
B	1.024	0.983	1.131	0.893	2.998	2.884	–	–	–
Fe^{3+}	–				–	–			0.079
Fe^{2+}	0.250	0.247	1.06	0.996	0.863	0.878	0.002	0.003	–
Mg	0.813	0.831	2.514	3.384	2.114	2.244	–	–	0.010
Mn	–	0.003	0.008	0.007	–	–	–	–	–
Ti	–	0.006	0.015	0.029	0.283	0.130	–	–	–
Cr	–	0.001	0.005	–	0.011	0.007	–	–	–
Ca	0.003	–	–	–	0.248	0.249	0.174	0.163	0.001
Na	–	–	–	0.030	0.673	0.694	0.717	0.773	0.006
K	–	–	–	–	0.022	0.022	0.111	0.047	–
F	–	–	0.265	0.249	0.244	0.195	–	–	–
Cations	6.030	6.027	14.533	14.844	20.100	20.087	4.99	4.97	12.07
Mg	76.5	77.1	70.4	70.6	70.9	71.8	–	–	11.4

Fluorine contents are assumed to be negligible in grandidierite calculations, **Chlorine contents are assumed to be negligible in grandidierite, kornerupine and tourmaline calculations, † all Fe is given as Fe^{2+}. For tourmaline analyses: incl. = inclusion tourmaline ($tourm_1$) within kornerupine, corona = $tourm_2$ corona growth on grandidierite. Sillimanite analysis — average of three points on one grain.

of Earth Sciences, University of Melbourne. The working beam conditions were 25 nA beam current and 10 μm beam width for both borosilicates and non-borosilicates. An accelerating voltage of 10 Kv and a PC2 detection crystal was utilized for B analysis. Elemental boron was utilised for the calibration standard for B analysis. For the remainder of the elements analysed, an accelerating voltage of 15 Kv was utilized, employing TAP (for elemental F, Na, Mg, Al and Si), PET (Cl, K, Ca, Ti and Mn) and LIF (Fe, Zn and Cr) detection crystals. Data were reduced via the Cameca PAP matrix correction program (Pouchou and Pichoir, 1984).

A number of problems have been recognized with the use of electron microprobe for detecting low atomic weight elements such as B, including peak shifts, interference caused by overlaps of higher order X-ray lines and low count yields (McGee et al., 1991). However, since the wt.% of B_2O_3 in grandidierite is fixed by stoichiometry at ~ 12 wt.% (E. Grew, pers. comm) for Mg-grandidierite, are considered a measure of the quality of the analyses. Representative mineral analyses for both localities are presented in Tables 1 and 2.

McCarthy Point locality. Grandidierite compositions are homogenous, with no zoning detected from

TABLE 2. Mineral analyses from Seal Cove

Oxide	garnet a	cordierite b	spinel c	plagioclase d	biotite e	grandidierite f	grandidierite g	kornerupine h	kornerupine i	kornerupine j	plagioclase k	plagioclase l	spinel m	spinel n	biotite o
SiO_2	37.21	50.01	0.01	61.42	36.05	19.74	19.72	29.19	28.94	29.51	60.93	60.42	0.00	0.03	36.42
Al_2O_3	21.69	33.74	55.62	23.80	14.83	51.20	50.85	38.22	39.73	39.26	23.85	24.36	53.98	57.01	14.90
TiO_2	0.02	0.01	0.02	0.04	4.88	0.00	0.00	0.19	0.23	0.05	0.01	0.02	0.00	0.00	6.21
MnO	1.34	0.06	0.10	0.01	0.01	0.03	0.06	0.14	0.14	0.15	0.03	0.00	0.20	0.15	0.01
FeO	31.67	5.78	33.33	0.06	14.62	6.85	6.96	13.29	13.39	11.81	0.02	0.03	39.00	37.00	17.11
MgO	6.42	10.19	6.98	0.00	14.05	10.36	10.55	12.34	12.43	12.76	0.00	0.00	5.11	5.37	11.87
CaO	1.49	0.01	0.00	6.00	0.00	0.00	0.00	0.00	0.07	0.05	6.08	6.19	0.00	0.00	0.02
ZnO	0.00	0.00	0.26	0.00	0.00	0.00	0.00	0.00	0.00	0.00	0.00	0.06	0.45	0.41	0.00
K_2O	0.00	0.06	0.00	0.51	10.00	0.00	0.00	0.00	0.00	0.03	0.57	3.13	0.02	0.00	9.92
Na_2O	0.05	0.02	0.01	7.81	0.17	0.00	0.00	0.00	0.04	0.00	7.78	5.68	0.02	0.01	0.03
B_2O_3	n.d.	n.d.	n.d.	n.d.	n.d.	11.64	12.16	3.62	4.64	3.48	n.d.	n.d.	n.d.	n.d.	n.d.
F	0.05	0.00	0.00	0.02	1.75	n.d.	n.d.	n.d.	n.d.	n.d.	0.00	0.00	0.05	0.00	1.49
Cl	0.00	0.00	0.00	0.00	0.10	n.d.	n.d.	n.d.	n.d.	n.d.	0.00	0.06	0.01	0.01	0.40
Total	99.97	99.91	96.33	99.67	96.50	99.82	100.30	96.99	99.61	97.10	99.27	99.95	98.85	99.98	98.38
No of O	12	18	32	8	22	9	9	22	22	22	8	8	32	32	22
Si	2.920	5.010	0.003	2.740	5.350	0.982	0.972	3.887	3.737	3.899	2.730	2.713	–	–	5.356
Al	2.010	3.980	15.106	1.250	2.594	2.995	2.957	6.000	6.047	6.111	1.260	1.289	14.600	15.120	2.582
B	–	–	–	–	–	0.996	1.035	0.832	1.039	0.794	–	–	–	–	–
Fe^{3+}	0.160	–	0.886	–	–	–	–	–	–	–	–	–	1.460	0.870	–
Fe^{2+}	1.920	0.480	5.537	–	1.815	0.283	0.287	1.480	1.442	1.301	–	–	6.030	6.090	2.104
Mg	0.750	1.520	2.398	–	3.109	0.773	0.776	2.449	2.388	2.508	–	–	1.750	1.800	2.602
Ca	0.130	–	–	0.290	–	–	–	–	0.008	0.008	0.290	0.298	–	–	0.003
Na	0.010	–	0.003	0.680	0.049	–	–	–	–	–	0.680	0.494	0.010	–	0.009
K	–	–	–	0.030	1.893	–	–	–	–	–	0.030	0.179	0.010	–	1.861
Ti	–	–	0.003	–	0.545	–	–	0.064	0.024	0.008	–	–	–	–	0.687
Mn	0.090	–	0.020	–	–	0.001	0.003	0.016	0.016	0.016	–	–	0.040	0.030	–
Zn	–	–	0.045	–	–	–	–	–	–	–	–	–	0.080	0.070	–
F	–	–	–	–	0.821	n.d.	n.d.	n.d.	n.d.	n.d.	–	–	–	–	0.693
Cl	–	–	–	–	0.025	n.d.	n.d.	n.d.	n.d.	n.d.	–	–	–	–	0.100
Cations	8.00	11.01	24.00	4.99	15.36	6.03	6.03	14.73	14.70	14.65	4.99	4.98	24.00	24.00	16.00
Mg	28.2	75.9	30.2	–	63.1	72.9	72.8	62.1	62.1	65.6	–	–	22.48	22.80	55.30

F and Cl contents were not determined (n.d.) for grandidierite and kornerupine, both assumed negligible for kornerupine, F contents assumed to be ~ 0.6 wt.% (based on Table 1 kornerupine F contents). Analyses a–j selected mineral analyses from segregation phases, analyses k–o selected minerals analyses of host gneiss phases.

core to rim in individual crystals. B_2O_3 contents are 12.0 wt.% and X_{Mg} [= atomic Mg/(Mg + Fe)] are 76.5–77.5. Individual kornerupine crystals are unzoned and compositions vary little between grains. B_2O_3 contents are relatively high (4.2–5.2 wt.% B_2O_3) compared with recently published kornerupine analyses (e.g. Waters and Moore, 1985; Grew et al., 1990; Grew et al., 1991b). F contents are typically $\sim$ 0.5 wt.% and there is negligible Cl. X_{Mg} varies little, ranging between 70.0 and 70.6.

The dominant tourmaline variety (T_2) varies little in composition. Compositions are dravitic with X_{Mg} between 70.1 and 71.8. Where T_2 occurs in the neck of boudinaged kornerupines is slightly more Mg-rich (74.8). Tourmaline that occurs as rounded inclusions in kornerupine and grandidierite (T_1) is similar in composition to T_2. The B_2O_3 contents are in the order of 10 wt.%.

Rare highly corroded grains of sillimanite contain around 1 wt.% of Fe_2O_3, and 0.06 wt.% MgO, and boron was generally not detected, although sillimanite can contain significant B_2O_3 at high temperatures and low a_{H_2O} (Grew and Hinthorne, 1983). Plagioclase from the host quartzofeldspathic gneisses are unzoned and are typically around An_{17}.

The Mg-Fe phases arranged in order of decreasing X_{Mg} are grandidierite ($X_{Mg} \sim$ 76–77), tourmaline$_2$ ($X_{Mg} \sim$ 72–75), tourmaline$_1$ and/or kornerupine ($X_{Mg} \sim$ 70).

Seal Cove locality. Coarse cordierite, biotite$_2$, kornerupine and early corroded phases (garnet, ilmenite, spinel and biotite$_1$) in the metamorphic segregations are generally uniform in composition. Resorbed garnets are almandine-rich ($\sim$ 67 mole %), with low grossular and spessartine contents ($\sim$ 2.8 and 4.0 mole %, respectively). Spinel contains around 70 mole % hercynite with an insignificant gahnite component. Spinel also typically contains $\sim$ 20% magnetite as an exsolution feature.

Both kornerupine and grandidierite are similar in composition to the McCarthy Point locality, although both have slightly lower X_{Mg} (cf. McCarthy Point values, kornerupine $X_{Mg} \sim$ 70 and grandidierite $X_{Mg} \sim$ 76).The phases within the metamorphic segregations at Seal Cove can be arranged in order of increasing X_{Mg} with garnet ($X_{Mg} \sim$ 28), hercynitic spinel ($X_{Mg} \sim$ 30), kornerupine ($X_{Mg} \sim$ 62—66), biotite$_{1,2}$ ($X_{Mg} \sim$ 63), grandidierite ($X_{Mg} \sim$ 73), and cordierite ($X_{Mg} \sim$ 75).

Plagioclase crystals within the felsic gneiss that hosts the segregations (matrix plagioclase) show minimal zoning, with individual compositions in the range An_{28-33}. Biotite compositions show more variation compared to other Fe-Mg matrix phases and less Mg-rich than biotite$_{1,2}$ found within the segregations. Typically matrix biotite is TiO_2-rich

(4.1–6.2 wt.%), F and Cl contents are generally 1.3–1.5 and 0.4–0.5 wt.% respectively. X_{Mg} ranges between extremes 52 and 59, but more commonly in the range 54–55. Matrix spinel is hercynitic with X_{Mg} around 22–23. Plagioclase compositions in the plagioclase domains around the multimineralic Mg-rich segregation cores are around $\sim An_{29}$.

$P–T$ conditions of grandidierite formation in Larsemann Hills

In order to assess the $P–T$ conditions of coexisting grandidierite-kornerupine at Seal Cove, phases that coexist with grandidierite and kornerupine are used in average pressure calculations. We utilize the quantitative average $P–T$ approach described by Powell and Holland (1994), using the expanded internally consistent thermodynamic dataset of Holland and Powell (1990).

Texturally early phases within the segregations (garnet, spinel, biotite$_1$, ilmenite, quartz$_1$ and sillimanite) partially destabilized to form cordierite, grandidierite, kornerupine and biotite$_2$. Quartz$_1$ and sillimanite (included in the $P–T$ calculations) although originally part of the early assemblage, were largely consumed during the formation of the later assemblage, and are now present as rare relict inclusion phases in host gneiss plagioclase.

The quantitative average $P–T$ technique of Powell and Holland (1994) searches for a set of independent reactions between the various end-members of minerals within an equilbrium assemblage. A χ^2 test is employed to quantify the reliability of the calculated answer which is expressed as a 'fit' value (σ_{fit}). The test is passed if σ_{fit} is less than maximum allowable from the χ^2 test at the 95% confidence level (Powell and Holland, 1994). The recognition of an equilibrium assemblage is of critical importance in employing this technique. We have utilized compositions of mineral phases within the segregations, assuming that these phases represent an equilibrium assemblage. The notable absence of Mg-Fe compositional zoning in segregation phases supports this assumption. Grandidierite and kornerupine are not used in the calculations due to the lack of thermodynamic data on these minerals. The thermodynamic mole fractions of end-members of each of the mineral phases are calculated (selected mineral analyses are presented in Table 2) and the activity uncertainties are the defaults suggested by Powell and Holland (1990).

The application of the average pressure approach can be affected by Fe—Mg re-equilibration exchange during cooling (e.g. Clarke and Powell, 1991) which can affect mineral compositions. This is particularly so for spinels from the segregations at Seal Cove that have exsolved $\sim$ 20% magnetite on cooling. The

TABLE 3. Summary of average pressure calculations using the methods and computer program THERMOCALC of Powell and Holland (1993) and the extended thermodynamic dataset of Holland and Powell (1988)

End Members	crd	fcrd	phl	ann	sp	py	alm	q	sill
Activity (a)	0.059	0.060	0.132	0.026	0.192	0.017	0.266	1.000	1.000
σ	0.05167	0.34262	0.24343	0.44458	0.19586	0.49570	0.1500	0	0

Independent reactions generated

  1) $2sp + 5q = crd$
  2) $py + 2sill = crd + sp$
  3) $phl + alm + 2sill = crd + ann + sp$
  4) $2ann + 3py + 6sill = 3fcrd + 2phl + 3sp$

Average calculated pressures for activity of $H_2O = 0.3$

				Calculated pressures at 750°C for individual reactions

					$P_{750°C}$	σ	ln K
@700°C = 5.2 kbar	$\sigma = 0.32$	σfit = 0.7	1)		5.3 kbar	0.96	2.764
@750°C = 5.5 kbar	$\sigma = 0.34$	σfit = 0.9	2)		4.8 kbar	0.81	1.880
@800°C = 5.7kbar	$\sigma = 0.39$	σfit = 1.1	3)		5.4 kbar	0.81	−2.474
			4)		5.5 kbar	1.07	2.020

Average calculated pressures for activity of $H_2O = 0.2$ Calculated pressures at 750°C for individual reactions

					$P_{750°C}$	σ	ln K
@700°C = 5.0 kbar	$\sigma = 0.32$	σfit = 0.7	1)		5.0 kbar	0.96	2.764
@750°C = 5.2 kbar	$\sigma = 0.34$	σfit = 0.9	2)		4.6 kbar	0.81	1.880
@800°C = 5.5kbar	$\sigma = 0.38$	σfit = 1.1	3)		5.2 kbar	0.81	−2.474
			4)		5.3 kbar	1.07	2.020

Mineral chemical data from Table 2. Activity uncertainties are the defaults as suggested by Powell and Holland (1993). For both conditions ($a_{H_2O} = 0.2$ and 0.3) a 95% confidence level is attained if σ_{fit} is less than 1.61. End-member abbreviations: crd = $Mg_2Al_4Si_5O_{18}$; fcrd = $Fe_2Al_4Si_5O_{18}$; phl = $KMg(Mg_2)Si[SiAl]O_{10}(OH)_2$; ann = $KFe(Fe_2)Si_2[SiAl])_{10}(OH)_2$; sp = $MgAl_2O_4$; py = $Mg_3Al_2Si_3O_{12}$; alm = $Fe_3^{3+}Al_2Si_3O_{12}$; q = SiO_2; sill = Al_2SiO_5.

proportion of exsolved magnetite:spinel was estimated visually in thin section. In order to consider the activity of spinel prior to exsolution, 20% magnetite is re-integrated into spinel. Magnetite is simplistically assumed to contribute a dilutional effect on the activity of spinel. Other phases within the segregations are assumed to have been minimally affected by post-metamorphic re-equilibration during cooling, and, again, the lack of significant compositional zoning across all segregation Fe-Mg phases supports this.

The temperature range selected ($\sim$ 750°C) is considered reasonable based on the extent of migmatization within the terrain, and by previous geothermometry, from the Larsemann Hills (Stüwe and Powell, 1989; Ren *et al.*, 1992). The activity of H_2O is assumed to be between 0.2 and 0.3, based on reported low a_{H_2O} from other granulite terrains (e.g. Edwards and Essene, 1988; Lamb and Valley, 1988)

and the extent of regional partial melting, which will reduce a_{H_2O} in the rock (Lamb and Valley, 1988).

Based on the above parameters, the average pressure calculations indicate conditions of formation for mineral phases coexisting with grandidierite-kornerupine to be between 5.2 $\pm$ 0.3 kbar at $a_{H_2O} = 0.2$, to 5.5 $\pm$ 0.3 kbar at $a_{H_2O} = 0.3$.

The details of the calculations are summarized in Table 3, and presented in Fig. 6.

Discussion

P–T conditions of coexisting grandidierite and kornerupine. The stable coexistence of grandidierite with kornerupine at Seal Cove and at McCarthy Point suggests the stability field of grandidierite can overlap with that of B-kornerupine (Robbins and Yoder, 1962; Werding and Schrey er, 1978). This is consistent with predictions from the schematic
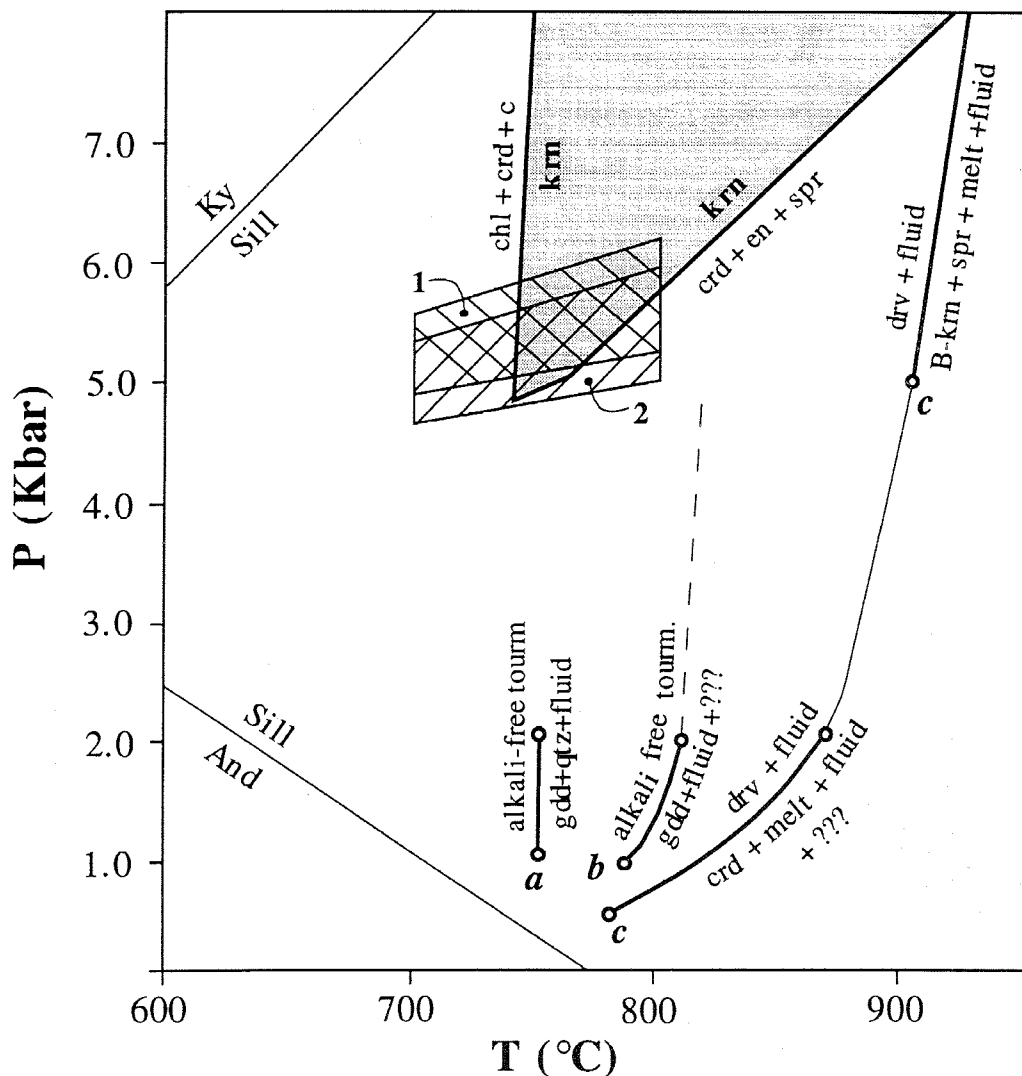
FIG. 6. Shaded boxes represents results of average P calculations from THERMOCALC between 700 and 800°C for the Seal Cove assemblages (box 1 $a_{H_2O} = 0.3$, box 2 $a_{H_2O} = 0.2$). Stippled area = field of stability of boron-free kornerupine as defined by Seifert (1975). Aluminium silicate stability field after Holdaway (1971). The stability field of B-kornerupine is likely to extend to higher temperatures and lower pressures relative to that of B free kornerupine (Seifert, 1975). Lines a, b and c represent results of various stability experiments on B-bearing phases (Sources of data: (a) Rosenberg and Foit (1975), (b) Werding and Schreyer (1984), (c) Robbins and Yoder (1962)). Mineral abbreviations; drv = Mg-tourmaline, melt = silicate melt, chl = chlorite, en = enstatite, spr = sapphirine, c = corundum.

pressure–temperature grid in the system KNFMA SHB ($P_{H_2O} < P_{total}$) constructed by Lonker (1988) and is confirmed by average pressure calculations which indicate that grandidierite–kornerupine assemblages can coexist at ~ 5.2 to 5.5 kbar at 750°C.

Sources of boron in Larsemann Hills. In the southwestern Larsemann Hills decimeter-thick psammitic gneisses with ~ 10–15 modal% kornerupine can be intermittently traced for several kilometres, suggesting that the original sedimentary sequence contained

units with significant boron. The McCarthy Point locality occurs close to kornerpine-rich units, suggest that the source of boron may be a primary compositional feature. This is supported by the distribution of the borosilicate assemblages at McCarthy Point where the borosilicates are restricted to a single layer several metres thick that can be traced for several hundred metres. However, at Seal Cove, the style of borosilicate occurrence, for example, as overgrowths on the early borosilicate absent assemblage, and the sporadic distribution of the borosilicates, more likely reflects boron infiltration and mobilization from a source external to the local host lithology.

Timing of borosilicate growth. At Seal Cove, the majority of borosilicate-bearing segregat: is clearly post-date S_2, implying borosilicate growth post-dates D_2. Kornerupine growth at McCarthy Point locally forms a moderately developed axial planar fabric to F_3 fold structures that formed in association with regionally extensive D_3 normal shearing. This suggests kornerupine growth pre-dated or was synchronous with D_3. Given that D_3 is coeval with, and post-dated by, near-isothermal decompression textures that formed at around 4.5 kbar and 750°C (Stüwe and Powell, 1989), the McCarthy Point borosilicates are inferred to have grown at pressures greater than 4.5 kbar. This is consistent with the calculated pressures of $\sim 5.2-5.5$ kbar for the Seal Cove borosilicate assemblages. Therefore, the growth of grandidierite and kornerupine is inferred to have post-dated peak metamorphism and occurred early in the near-isothermal decompression retrograde $P-T$ history in the Larsemann Hills.

Acknowledgements

References

Ackermand, D., Windley, B. F., and Razafiniparany, A. H. (1991) Kornerupine breakdown textures in paragneisses from southern Madagascar. *Mineral. Mag.,* **55**, 71–80.

Black, L. P., Harley, S. L., Sun, S. S., and McCulloch, M. T. (1987) The Rayner Complex of East Antarctica: Complex isotopic systematics within a Proterozoic mobile belt. *J. Metam. Geol.,* **5**, 1–26.

Black, P. M. (1970) Grandidierite from Cuvier Island, New Zealand. *Mineral. Mag.,* **37**, 615–7.

Carson, C. J., Dirks, P. H. G. M., Hand, M., Sims, J. P., and Wilson, C. J. L. (1995) Compressional and extensional tectonics in low-medium pressure granulites from the Larsemann Hills, East Antarctica. *Geol. Mag.* (in press).

Clarke, G. L. and Powell, R. (1991) Proterozoic granulite facies metamorphism in the southeastern Reynolds Range, Central Australia: geological context, $P-T$ path and overprinting relationships. *J. Metam. Geol.,* **9**, 267–81.

de Roever, E. W. F. and Kieft, C. (1976) Grandidierite of contact-metamorphic origin from Maratakka, north west Surinam. *Amer. Mineral.,* **61**, 332–3.

Dirks, P. H. G. M., Carson, C. J., and Wilson, C. J. L. (1993) The deformational history of the Larsemann Hills, Prydz Bay: the importance of the Pan-African (500 Ma) in East Antarctica. *Antarctic Sci.,* **5**, 179–92.

Edwards, R. L. and Essene, E. J. (1988) Pressure, temperature and C–O–H fluid fugacities across the amphibolite–granulite transition, Northwest Adirondack Mountains, New York. *J. Petrol.,* **29**, 39–72.

Grew, E. S. (1982) Kornerupine and boron in high-grade metamorphic rocks. *Geol. Soc. Am. Abstr. with Programs,* **14**, 502.

Grew, E. S. and Hinthorne, J. R. (1983) Boron in sillimanite. *Science,* **221**, 547–9.

Grew, E. S., Yates, M. G., Beryozkin, V. I. and Kitsul, V. I. (1989) Secondary grandidierite in kornerupine-sapphirine rocks of the Aldan Shield. *Dokl. Akad. Nauk. SSSR,* **309**, 423–8 (in Russian).

Grew, E. S., Chernosky, J. H., Werding, G., Abraham, K., Marquez, N. and Hinthorne, J. R. (1990) Chemistry of kornerupine and associated minerals, wet chemical, ion microprobe, and X-ray study emphasizing Li, Be, B, and F contents. *J. Petrol.,* **31**, 1025–70.

Grew, E. S., Yates, M. G., Beryozkin, V. I. and Kitsul, V. I. (1991*a*) Kornerupine in slyudites from the Usman River Basin on the Aldan Shield: Part I. Geology and petrography. *Soviet Geol. Geophysics.,* **32**, 66–74.

Grew, E. S., Yates, M. G., Beryozkin, V. I. and Kitsul, V. I. (1991*b*) Kornerupine in slyudites from the Usman River Basin on the Aldan Shield: Part II. Chemistry of the minerals, mineral reactions. *Soviet Geol. Geophysics,* **32**, 85–98.

Haslam, H. W. (1980) Grandidierite from a metamorphic aureole near Mchinji, Malawi. *Mineral. Mag.,* **43**, 822–3.

Helmers, H. and Lustenhouwer, W. J. (1988) Grandidierite from the Comrie aureole. *Scottish J. Geol.*, **24**, 245–8.

Holdaway, M. J. (1971) Stability of andalusite and sillimanite and the aluminium silicate phase diagram. *Amer. J. Sci.*, **271**, 97–131.

Holland, T. J. B. and Powell, R. (1990) An enlarged and updated internally consistent thermodynamic dataset with uncertainties and corrections: the system K_2O–Na_2O–CaO–MgO–MnO–FeO–Fe_2O_3–Al_2O_3–TiO_2–SiO_2–C–H_2–O_2. *J. Metam. Geol.*, **8**, 89–124.

Huijsmans, J. P. P., Barton, M. and van Bergen, M. J. (1982) A pegmatite containing Fe-rich grandidierite, Ti-rich dumortierite and tourmaline from the Precambrian, high grade metamorphic complex of Rogaland, S.W. Norway. *Neues Jahrb. Mineral. Abh.*, **143**, 249–61.

Krogh, E. (1975) The first occurrence of grandidierite in Norway. *Norsk. Geol. Tidsskr.*, **55**, 77–80.

Lamb, W. M. and Valley, J. W. (1988) Granulite facies amphibolite and biotite equilibria, and calculated peak-metamorphic water activities. *Contrib. Mineral. Petrol.*, **100**, 349–60.

Lonker, S. W. (1988) An occurrence of grandidierite, kornerupine and tourmaline in southeastern Ontario, Canada. *Contrib. Mineral. Petrol.*, **98**, 502–16.

McGee, J. J., Slack, J. F. and Herrington, C. R. (1991) Boron analysis by electron microprobe using MoB_4C layered synthetic crystals. *Amer. Mineral.*, **76**, 681–4.

Nicollet, C. (1990) Occurrences of grandidierite, serendibite and tourmaline near Ihosy, southern Madagascar. *Mineral. Mag.*, **54**, 131–3.

Olesch, M. and Seifert, F. (1976) Synthesis, powder data and lattice constants of grandidierite, $(Mg,Fe)Al_3BSiO_9$. *Neues Jahrb. Mineral. Mh.*, 513–18.

Pouchou, L. and Pichoir, F. (1984) A new model for quantitative X-ray microanalysis. *Reserche Aerospatiale*, **3**, 167–92.

Powell, R. and Holland, T. (1990) Calculated mineral equilibria in the pelite system, KFMASH (K_2O–FeO–MgO–Al_2O_3–SiO_2–H_2O). *Amer. Mineral.*, **75**, 367–80.

Powell, R. and Holland, T. J. B. (1994) Optimal geothermometry and geobarometry. *Amer. Mineral.*, **79**, 120–33.

Ren, L., Zhao, Y., Liu, X. and Chen, T. (1992) Re-examination of the metamorphic evolution of the Larsemann Hills, East Antarctica. In *Recent Progress in Antarctic Earth Science* (Y. Yoshida *et al.*, eds.) Terra Scientific Publishing Co., Tokyo, pp. 145–53.

Robbins, C. R. and Yoder, H. S. Jr. (1962) Stability relations of dravite, a tourmaline. *Carnegie Inst. Washington Yearbook*, **61**, 106–7.

Rosenburg, P. E. and Foit, F. F. Jr (1975) Alkali-free tourmalines in the system MgO–Al_2O_3–SiO_2–H_2O–B_2O_3. *Geol. Soc. Amer. Abstr. with Programs*, **7**, 1250–1.

Seifert, F. (1975) Boron-free kornerupine: A high pressure phase. *Amer. J. Sci.*, **275**, 57–87.

Sheraton, J. W., Offe, L. A., Tingey, R. J. and Ellis, D. J. (1980) Enderby Land, Antarctica — An unusual Precambrian high-grade metamorphic terrain. *Austral. J. Earth Sci.*, **27**, 1–18.

Sheraton, J. W., Black, L. P. and McCull och, M. T. (1984) Regional geochemical and isotopic character-istics of high-grade metamorphic of the Prydz Bay area: the extent of Proterozoic reworking of Archaean continental crust in East Antarctica. *Precambrian Res.*, **28**, 169–98.

Stüwe, K. and Powell, R. (1989) Low pressure granulite facies metamorphism in the Larsemann Hills area, East Antarctica; petrology and tectonic implications for the evolution of the Prydz Bay area. *J. Metam. Geol.*, **7**, 465–83.

van Bergen, M. J. (1980) Grandidierite from aluminous metasedimentary xenoliths within acid volcanics, a first record in Italy. *Mineral. Mag.*, **43**, 651–8.

Vrána, S. (1979) A polymetamorphic assemblage of grandidierite, kornerupine, Ti-rich dumortierite, tourmaline, sillimanite and garnet. *Neues Jahrb. Mineral. Mh.*, 22–33.

Waters, D. J. and Moore, J. M. (1985) Kornerupine in Mg-Al-rich gneisses from Namaqualand, South Africa: mineralogy and evidence for late-meta-morphic fluid activity. *Contrib. Mineral. Petrol.*, **91**, 369–82.

Werding, G. and Schreyer, W. (1978) Synthesis and crystal chemistry of kornerupine in the system MgO–Al_2O_3–SiO_2–B_2O_3–H_2O. *Contrib. Mineral. Petrol.*, **67**, 247–59.

Werding, G. and Schreyer, W. (1984) Alkali-free tourmaline in the system MgO–Al_2O_3–B_2O_3–SiO_2–H_2O. *Geochim. Cosmochim. Acta*, **48**, 1331–44.

Zhao, Y., Song, B., Wang, Y., Ren, L., Li, J. and Chen, T. (1992) Geochronology of the late granite in the Larsemann Hills, East Antarctica. In *Recent Progress in Antarctic Earth Science* (Y. Yoshida *et al.*, eds.) Terra Scientific Publishing Co., Tokyo, pp. 155–61.